ACS OMEGA

http://pubs.acs.org/journal/acsodf

Article

Gallium−Curcumin Nanoparticle Conjugates as an Antibacterial Agent against *Pseudomonas aeruginosa*: Synthesis and Characterization

Gopika Ramesh, Jyothi Embekkat Kaviyil, Willi Paul, Renjith Sasi, and Roy Joseph*

Cite This: *ACS Omega* 2022, 7, 6795−6809

Read Online

ACCESS | Metrics & More | Article Recommendations | Supporting Information

ABSTRACT: Combating antibiotic resistance has found great interest in the current clinical scenario. *Pseudomonas aeruginosa*, an opportunistic multidrug-resistant pathogen, is well known for its deadly role in hospital-acquired infections. Infections by *P. aeruginosa* are among the toughest to treat because of its intrinsic and acquired resistance to antibiotics. In this study, we project gallium−curcumin nanoparticle (GaCurNP) conjugates as a prospective candidate to fight against *P. aeruginosa*. The synthesized GaCurNPs were spherical with an average size ranging from 25−35 nm. Analysis by Fourier transform infrared (FT-IR) spectroscopy, Raman spectroscopy, and X-ray photoelectron spectroscopy deduced the nature of interaction between gallium and curcumin. Conjugate formation with gallium was found to improve the stability of curcumin at the physiological pH. When tested after 24 h of contact, at the physiological pH and 37 °C, the degradation of curcumin bound in the GaCurNPs was 26%, while that of native curcumin was 95%. The minimum inhibitory concentration (MIC) of GaCurNPs was found to be 82.75 μg/mL for *P. aeruginosa* (*ATCC* 27853). GaCurNPs also showed excellent biofilm inhibition at 4MIC concentration. Raman spectroscopic analysis showed that GaCurNPs are capable of disrupting the cells of *P. aeruginosa* within 3 h of contact. Live/dead imaging also confirmed the compromised membrane integrity in cells treated with GaCurNPs. Scanning electron microscopy analysis showed membrane lysis and cell structure damage. The AlamarBlue assay showed that when L929 cell lines were treated with GaCurNPs with concentrations as high as 350 μg/mL, the cell viability elicited by the nanoparticles was 70.89%, indicating its noncytotoxic nature. In short, GaCurNPs appear to be a promising antibacterial agent capable of fighting a clinically significant pathogen, *P. aeruginosa*.

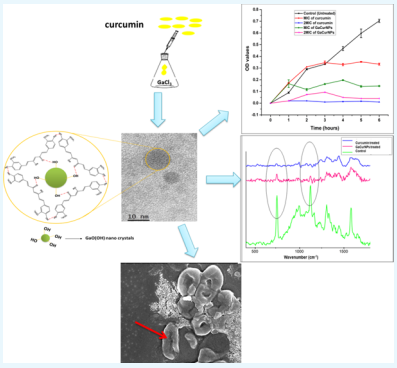

1. INTRODUCTION

Antibiotic resistance is one of the major challenges faced by the human race in recent times. The overuse and abuse of antibiotics are the major reasons for this resistance globally.[1] Antibiotic resistance is acquired by bacteria via different means. The mechanisms of antibiotic resistance include modification of antibiotics, i.e., the addition of specific chemical moieties or destruction of the antibiotic molecules itself, restricted uptake and efflux, resistance owing to global cell adaptive process, and bypass of target sites.[2] One of the toughest antibiotic-resistant bacteria is the Gram-negative rod-shaped bacterium called *Pseudomonas aeruginosa*. It is not frequently found as part of normal human microflora and is an opportunistic pathogen.[3] It causes urinary tract infections, respiratory tract infections, dermatitis, soft tissue infections, gastrointestinal infections, and even bone and joint infections. *P. aeruginosa* is predominantly isolated from cystic fibrosis patients. It is also one of the major organisms that form biofilms in medical devices.[4,5] *P. aeruginosa* is resistant to many classes of antibiotics due to intrinsic, acquired, and genetic factors.[6] Intrinsic factors include outer membrane impermeability, genetic capability to express resistance mechanisms, mutation in chromosomal genes that regulate resistance genes, and acquisition of resistance genes through plasmids and bacteriophages. The resistance of *P. aeruginosa* against antibiotics makes it tough to treat using many of the currently available antibiotics. Treatment of skin and soft tissue infections topically is also of concern owing to the increasing antibiotic resistance. Effective antibacterial compounds are need of the hour to mitigate and prevent infections caused by *P. aeruginosa*. Many alternatives to antibiotics have been investigated to fight against *P. aeruginosa*.[7−9] Use of antibacterial nanoparticles is considered to be a promising nonconventional therapy for fighting antibiotic-resistant bacteria owing to its excellent antibacterial activity.[10−13]

Curcumin, a polyphenolic compound isolated from the rhizome of *Curcuma longa*, is being used as a medicine for

Received: November 13, 2021
Accepted: February 8, 2022
Published: February 17, 2022

various ailments for ages. It exhibits antibacterial,[14] anticancer,[15] antioxidant,[16] anti-inflammatory,[17] antiviral, and anti-Alzheimer's activities.[18] Curcumin was found to be safe for humans with a daily dose of up to 12 000 mg.[19] It is also called *diferuloyl methane* and exists in nature along with its analogues, namely, demethoxycurcumin and bisdemethoxy curcumin, and together, they are called curcuminoids. Curcumin is the major component among the curcuminoids and is readily soluble in solvents such as methanol, ethanol, and dimethyl sulfoxide. It is insoluble in water at acidic and neutral pH conditions. It dissolves when the pH is alkaline. However, it degrades rapidly at the alkaline pH conditions.[20] Trans-6-(4′-hydroxy-3′-methoxyphenyl)-2,4-dioxo-5-hexenal was detected as the major degradation product of curcumin, whereas vanillin, ferulic acid, and feruloylmethane are the minor products when incubated in 0.1 M phosphate buffer (at pH 7.2 and at 37 °C). It was reported that metal−curcumin complexes were 20-fold more stable than curcumin and the degradation rate of curcumin was less than 5% *in vivo*.[21] In a green synthesis method, curcumin was used for the synthesis of gold nanoparticles. These nanoparticles showed hemocompatibility and were less cytotoxic.[22] A similar approach has been successfully used for the synthesis of silver nanoparticles, and these nanoparticles were found to possess antibiofilm activity against clinically important Gram-positive and Gram-negative bacterial strains.[23]

Curcumin nanoparticles of size range 2−40 nm, prepared by the wet-milling technique, were found to be effective against *Staphylococcus aureus*, *Bacillus subtilis*, *Escherichia coli*, *P. aeruginosa*, *Penicillium notatum*, and *Aspergillus niger*.[24] The broad-spectrum antibacterial nature of curcumin was attributed to its membrane damaging property. A comprehensive study by Tyagi et al. showed that the bactericidal activity of curcumin was brought about by membrane leakage.[25] Curcumin acts on both Gram-positive and Gram-negative bacteria, which confirms its broad-spectrum nature. The minimum inhibitory concentrations of curcumin for seven clinically important strains, including methicillin-resistant *S. aureus* and methicillin-sensitive *S. aureus*, *P. aeruginosa*, and *Klebsiella pneumoniae*, were determined and reported to be 219, 217, 175, and 216 μg/mL, respectively.[26] Carbocyclic curcumin analogue was reported to disrupt bacterial cell proliferation by destroying the Z-ring of FtsZ.[27] Curcumin coated with tannic acid and metal ions was found to have antibacterial effect on both *E. coli* and *S. aureus*.[28] Curcumin nanoparticles were found to inhibit sortase A, a bacterial surface protein anchoring transpeptidase, and curcumin was also found to inhibit attachment of *S. aureus* to fibronectin.[29]

P. aeruginosa is an innately antibiotic-resistant microorganism that plays a crucial role in hospital-based infections. Controlling the infections caused by *P. aeruginosa* is one of the greatest challenges faced in hospital settings. Biofilms of *P. aeruginosa* have been isolated from almost all medical devices ranging from catheters to hip prostheses.[30] Finding antibacterial agents and antibiotics that can effectively control the growth of these resistant organisms has become a clinical necessity. Mohammadi et al. reported a method for synthesizing gallium−curcumin complexes by refluxing gallium nitrate and curcumin with methanol as a solvent in the presence of triethylamine.[31] However, their product showed negligible antibacterial activity. Here, we report the development of gallium−curcumin nanoparticles (GaCurNPs) that possess effective antibacterial activity against *P. aeruginosa*. The particle-bound curcumin has improved stability at physiological pH with a very low rate of degradation. Gallium metal has been chosen owing to its nontoxicity. Further, citrate-buffered gallium nitrate is an FDA-approved drug for treating hypercalcemia. It was found to be very effective against *P. aeruginosa*. Combining the antibacterial effect of both gallium and curcumin in a nanoparticle form would be interesting and worth exploring.

2. RESULTS AND DISCUSSION

2.1. Size and ζ-potential. Particle size estimation by the dynamic light scattering (DLS) technique revealed that the average size of GaCurNPs was 79.5 nm (Figure 1a). DLS measures the hydrodynamic radius and hence this size will be slightly greater than the actual size of the particle. The ζ-potential of GaCurNPs was measured as +22.1 mV (Figure 1b), which indicated that the particles were moderately stable. Transmission electron microscopy revealed that the particles were spherical and the size ranged from 25 to 35 nm (Figure 1c,d). High-resolution transmission electron microscopy (HRTEM) revealed the crystalline fringes of GaCurNPs. The perfect crystalline pattern suggests the incorporation of gallium in GaCurNPs. This was further confirmed by the powder X-ray diffraction (XRD) analysis of GaCurNPs and curcumin (Figure 2a). Native curcumin gave the characteristic crystalline pattern as reported elsewhere.[32] However, in the case of GaCurNPs, the crystalline pattern of curcumin was replaced by the typical ordering of gallium oxides. JCPDS indexing of the crystalline pattern suggests the existence of Ga as GaO(OH) in the GaCurNPs. The absence of any crystalline fringes of curcumin and the presence of a broad halo in the lower angle region suggest the self-assembly of curcumin molecules around the GaO(OH) nanoparticles. The HRTEM image of GaCurNPs displayed lattice fringes separated by 0.43 nm, which is in good agreement with the d-spacing of 110 planes of GaO(OH) (Figure 1e). The selected area electron diffraction (SAED) pattern of the GaCurNPs also displayed the characteristic crystalline fringes of GaO(OH) (Figure 1f).

Formation of GaO(OH) nanoparticles from the aqueous solution of Ga^{3+} was reported earlier by Gedanken et al.[33] The stability of Ga-containing oxides like Ga_2O_3 and GaO(OH) can be improved by functionalization with ligands, especially with acidic functionalities. Such functionalization will also impart synergistic functional properties to the nanoparticles.[34] Herein, the enolic form of curcumin interacts with the *in situ* formed GaO(OH) to produce GaCurNPs.

2.2. FT-IR Spectroscopy. Vibrational spectroscopic analysis with FT-IR provided additional information about the chemical structure of GaCurNPs (Figure 2b). A detailed analysis of the vibrational spectral features of curcumin was reported by Kolev and co-workers.[35] In the spectrum of curcumin, the peak at 1626 cm^{-1} corresponds to the mixed vibration of carbonyl C═O and C═C. The peak at 1600 cm^{-1} indicated the symmetric aromatic stretching vibrations ν(C═C). The peak at 1506 cm^{-1} was due to the mixed vibrations such as C−O stretching, C−C−C bending, and C−C−O bending. The in-plane C−OH bending of the enolic group is responsible for the peak at 1427 cm^{-1}, while the enol ν(C−O) peak was obtained at 1272 cm^{-1}. The peaks at 1153 and 1025 cm^{-1} were attributed to the skeletal C−C−H and methyl group deformations, respectively. The enolic C−OH in-plane bending vibration was observed at 962 cm^{-1}, and out-of-plane bending vibrations of C−C−H moieties were observed at 855

https://doi.org/10.1021/acsomega.1c06398
ACS Omega 2022, 7, 6795−6809

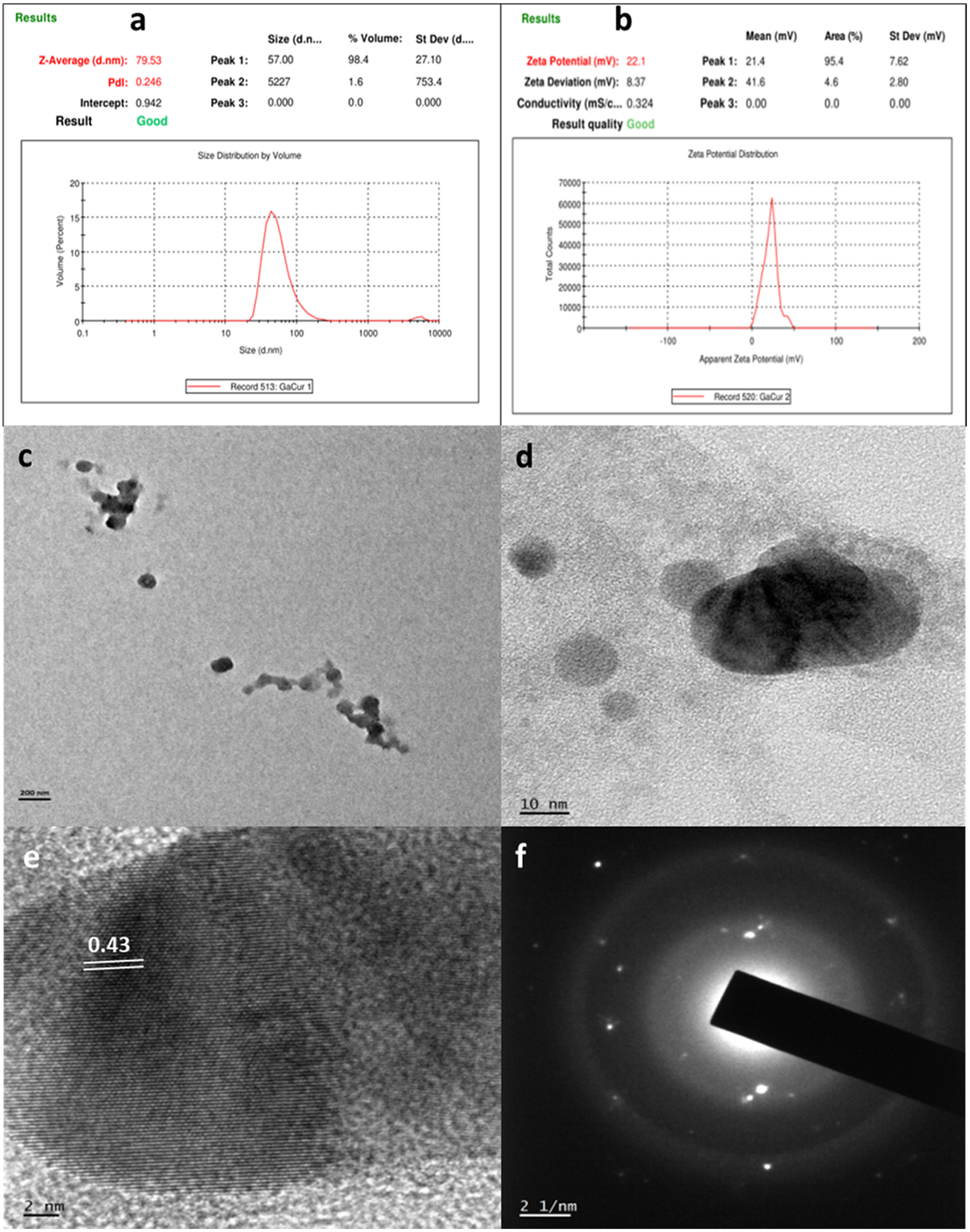

Figure 1. (a) Size of GaCurNPs measured by the dynamic light scattering technique, (b) ζ-potential of GaCurNPs, (c) transmission electron microscopy (TEM) image of GaCurNPs, (d) and (e) high-resolution TEM image of GaCurNPs, and (f) selected area electron diffraction pattern of GaCurNPs.

and 806 cm^{-1}. The multiplets observed in the region of 2840−3000 cm^{-1} were due to the aliphatic and aromatic C−H stretching vibrations (Figure 2c). Two distinct peaks were observed at 3320 and 3510 cm^{-1} corresponding to the enolic

https://doi.org/10.1021/acsomega.1c06398
ACS Omega 2022, 7, 6795−6809

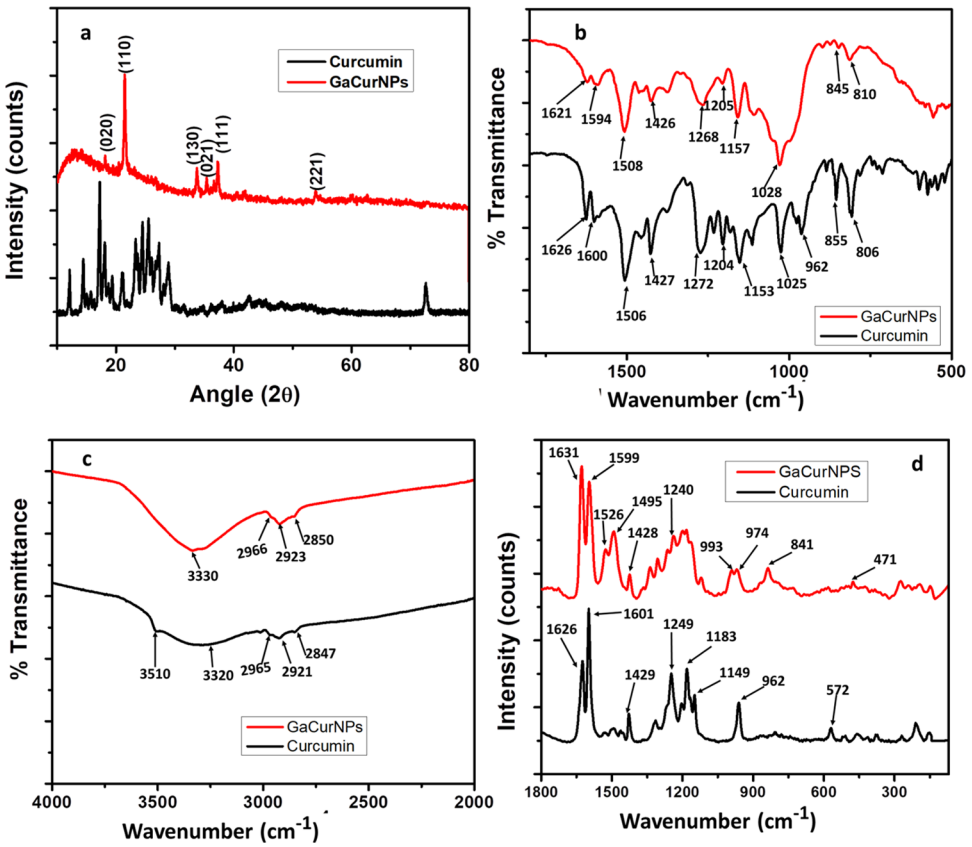

Figure 2. Comparison of spectral features of curcumin and GaCurNPs: (a) XRD pattern, (b, c) different wavenumber ranges of Fourier transform infrared (FT-IR) spectra, and (d) Raman spectra.

and phenolic O−H groups, respectively. In the spectrum of GaCurNPs, most of the peaks corresponding to the curcuminic structure were observed with a slight shift in the wavenumber and intensity due to the interaction with GaO(OH).[36] No characteristic bands of GaO(OH) were observed in the FT-IR spectrum possibly due to overlapping and chemical modification.[37] Unlike in curcumin, the O−H stretching of enolic and phenolic parts merged to form a broad peak centered at 3330 cm^{-1}. These observations suggest that GaCurNP has a core of GaO(OH) particles surrounded by hydrogen-bonded self-assembly of curcumin molecules.[38]

2.3. Raman Spectroscopy. Raman spectroscopy analysis provided a more vivid insight into the formation of GaCurNPs (Figure 2d). In the spectrum of curcumin, the strong peaks observed in the region of 1600 and 1630 cm^{-1} were assigned to the mixed vibrations of ν(C═O) and ν(C═C).[39] The strong peak at 1601 cm^{-1} was characteristic of the aromatic vibrations of the $C{=}C_{ring}$ and that at 1626 cm^{-1} corresponded to the C═O stretching vibrations. The peak at 1428 cm^{-1} indicated the presence of phenolic ν(C−O). The enolic ν(C−O) vibrations are marked as 1149 and 1183 cm^{-1}.

The Raman spectrum of the GaCurNPs clearly indicated the involvement of the enolic framework of curcumin in nanoparticle formation.[40] The relative intensities of C═O and C═C vibrations got reversed on moving from native curcumin to GaCurNPs. This suggests the active involvement of enolic groups in conjugate formation. The broadening of characteristic enolic peaks further illustrates the enolic involvement. Further enhancement of a peak at 1495 cm^{-1} corresponding to the aromatic C═C ring vibrations suggests the self-assembly of curcumin units with aromatic rings along the periphery during particle formation.[41] Further characteristic peaks corresponding to GaO(OH) were also observed in the Raman spectrum of GaCurNPs. The peak observed at 475 cm^{-1} corresponds to the Ga−O deformation peak of GaO(OH) units.[42] The presence of additional peaks at the lower wavenumber regime such as 841, 421, and 241.5 cm^{-1} may also be attributed to the interaction of GaO(OH) with curcumin.

2.4. X-ray Photoelectron Spectroscopy. The chemical identity of constituents and the nature of binding interactions were studied employing X-ray photoelectron spectroscopy (XPS). The XPS spectrum of GaCurNPs displays the characteristic peaks of GaO(OH) and curcumin, confirming their presence in the nanoparticles. Characteristic transitions of Ga are observed at 1146.51 (Ga $2p_{1/2}$), 1119.61 (Ga $2p_{3/2}$), 22.42 (Ga $3d_{3/2}$), and 20.51 eV (Ga $3d_{5/2}$), matching with the literature report.[43,44] Peaks observed at around 284 and 532 eV are ascribed to the carbon (C 1s) and oxygen (O 1s) atoms of curcumin. The comparison of C 1s and O 1s peaks of GaCurNPs with that of bare curcumin shows significant peak broadening, which may be attributed to the interaction between GaO(OH) and curcumin (Figure 3a). Deconvolution of the peaks provides more insight into the mode of interactions. The C 1s peak of curcumin is deconvoluted to three major peaks corresponding to sp^3 carbon (284.72 eV), C−O (286.23 eV), and C═O (288.28 eV). Interestingly, deconvolution of the broad C 1s peak of GaCurNPs yields four peaks and a mild shift in the peak positions is also observed. The fourth peak observed at 283.94 eV corresponds to the sp^2-hybridized carbon atom, suggesting the existence of curcumin in the enolic form in the complex. The oxygen peak (O 1s) of

https://doi.org/10.1021/acsomega.1c06398
ACS Omega 2022, 7, 6795−6809

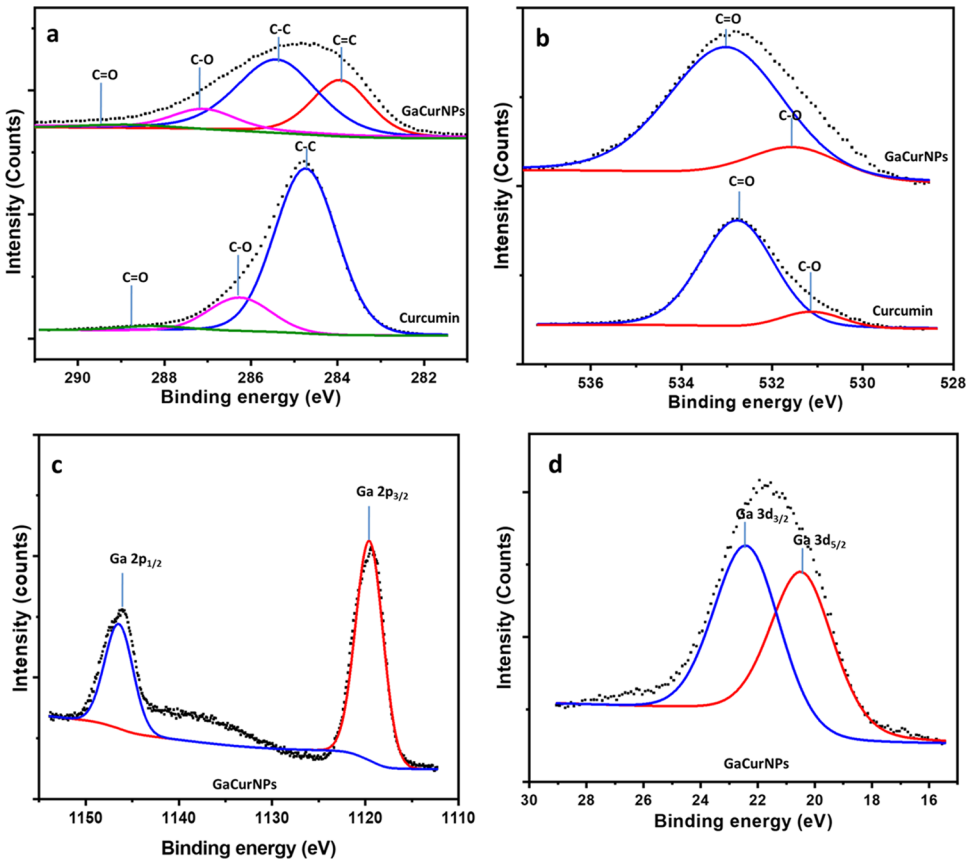

Figure 3. High-resolution XPS spectra of GaCurNPs and curcumin: (a) C 1s peaks of curcumin and GaCurNPs, (b) O 1s peaks of curcumin and GaCurNPs, (c) Ga 2p peaks of GaCurNPs, and (d) Ga 3d peaks of GaCurNPs.

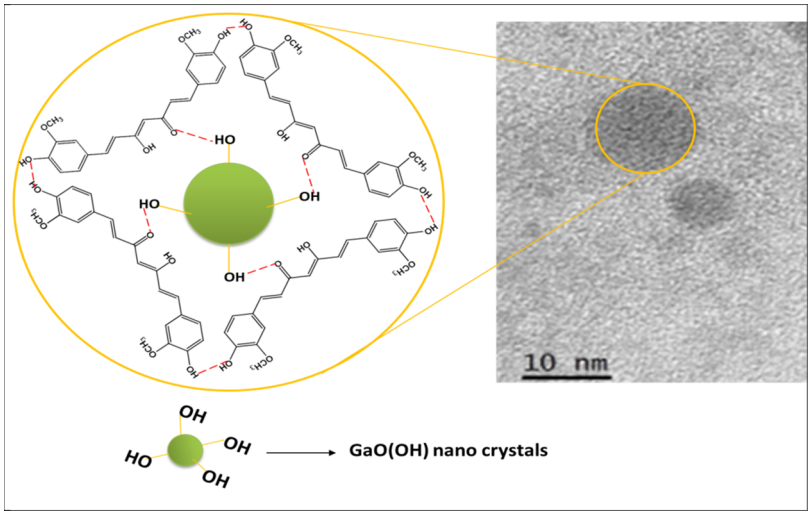

Figure 4. Schematic representation of the structure proposed for GaCurNPs.

pure curcumin was deconvoluted to C−O (531.18 eV) and C═O (532.77 eV) peaks (Figure 3b). In GaCurNPs, the O 1s spectrum retains identical peaks but the peak gets broadened due to the Ga−curcumin interactions. It was reported that O 1s peaks of GaO(OH) (Ga−OH and Ga^{3+}−O) also have their binding energy in this region.[45] So, there will be possible overlapping of the O 1s peaks of GaCurNPs.

From the FT-IR, Raman, and XPS analyses, it could be deduced that no coordinate or covalent bond was formed between gallium and curcumin in GaCurNPs. Also, XRD patterns and XPS binding energies of Ga indicate that Ga exists in the +3 oxidation state as in GaO(OH). The presence of hydroxyl groups on the surface of GaO(OH) enables it to establish hydrogen bonding with curcumin, which was confirmed by FT-IR analyses. The noncovalent interactions result in the self-assembly of curcumin molecules around GaO(OH) to form GaCurNPs. This noncovalent self-assembly would facilitate the release of curcumin to the medium, which favors curcumin dissolution. Based on the evidence obtained

https://doi.org/10.1021/acsomega.1c06398
ACS Omega 2022, 7, 6795−6809

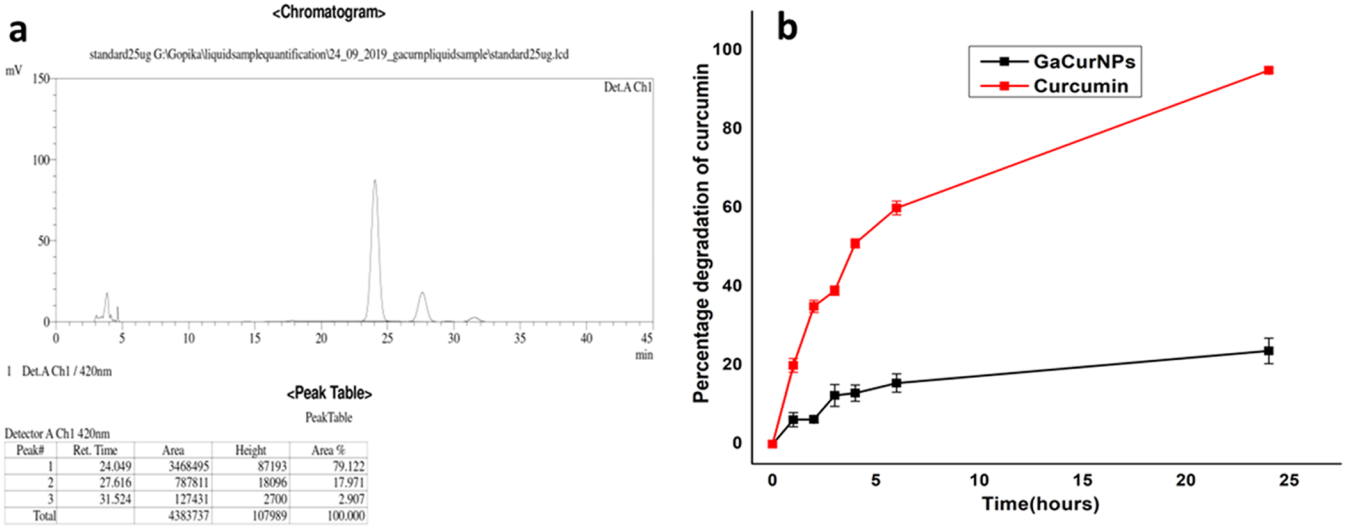

Figure 5. (a) Chromatogram of curcumin and (b) degradation profile of native curcumin and curcumin attached to GaCurNPs determined at 37 °C and pH 7.4.

Table 1. MIC Values of GaCurNPs and Curcumin against *P. aeruginosa* Strains

	MIC (μg/mL)		MBC (μg/mL)		
P. aeruginosa strains	curcumin	GaCurNPs	curcumin	GaCurNPs	susceptibility to Carbapenems and Colistin
ATCC 27853	41.37	82.75	82.75	165	susceptible
clinical strain 1	50	100	100	200	susceptible
clinical strain 2	100	200	200	400	resistant
clinical strain 3	100	100	200	200	susceptible
clinical strain 4	50	100	100	200	susceptible

by spectroscopic and XRD analyses, the structure illustrated in Figure 4 is proposed for GaCurNPs.

2.5. Curcumin Content in GaCurNPs. The amount of curcumin per milligram of GaCurNPs was estimated by reverse-phase high-performance liquid chromatography (RP-HPLC). Curcumin was a mixture of three active analogues—curcumin, demethoxycurcumin, and bisdemethoxy curcumin (Figure 5a)—and their ratio was found to be 79:18:3. The retention times of the components were 24.0, 27.6, and 31.5 min. The curcumin bound to the particles was extracted in ethanol and quantified using the calibration curve. It was estimated that 1 mg of GaCurNPs contains 200 ± 3.7 μg of curcumin (n = 3).

2.6. Stability of Curcumin Present in GaCurNPs at Physiological pH. Curcumin degrades rapidly at physiological pH (7.4) with a degradation constant of 0.0145 min^{-1} or 0.924 h^{-1}.[46] Both curcumin and GaCurNPs were incubated in conditions mimicking physiological conditions as described in Section 4.5. Curcumin was extracted in ethanol and loaded into the HPLC column. The results revealed that the curcumin bound to the GaCurNPs was relatively stable at physiological conditions compared to native curcumin. At 1 h itself, the degradation rate of native curcumin was 21%, whereas in GaCurNPs, the degradation rate of bound curcumin was only 6.2%. As time progressed, the degradation escalated at a faster rate for native curcumin, reaching 63% degradation at 6 h. GaCurNP-bound curcumin degraded very slowly and recorded only 23.4% degradation at 24 h, whereas native curcumin showed 95.5% degradation at 24 h. The typical HPLC chromatogram of curcumin and the degradation kinetics of native curcumin and GaCurNPs are given in Figure 5.

2.7. Antibacterial Activity of GaCurNPs on *P. aeruginosa*. *2.7.1. Minimum Inhibitory Concentration (MIC) and Minimum Bactericidal Concentration (MBC) of GaCurNPs by the Microbroth Dilution Method.* The MICs of curcumin and GaCurNPs against *P. aeruginosa* were determined using a range of concentrations. The concentrations tested were 662, 331, 165.5, 82.75, 41.375, 20.68, and 10.34 μg/mL. The MIC values obtained for curcumin and GaCurNPs against *P. aeruginosa* were 41.37 and 82.75 μg/mL, respectively. The results were confirmed by two independent experiments done in triplicates for all of the concentrations analyzed. MBC was determined as the lowest concentration at which there was no appearance of colonies when transferred from broth to agar plates. In MIC, bacterial growth appeared even though there was no growth in microbroth dilution assays. The previously found MIC values of curcumin against *P. aeruginosa* (ATCC 27853) was 175 μg/mL by Gunes et al.[26] The MIC of curcumin against *P. aeruginosa* (ATCC 25619) was estimated to be 512 μg/mL by Yadav et al.[47] The subinhibitory concentration of curcumin against *P. aeruginosa* PAO1 was determined as 125 μg/mL.[48] MIC values were also determined for four clinical isolates of *P. aeruginosa*, and these ranged from 50 to 200 μg/mL. The MIC values obtained for all of the strains tested are compiled in Table 1. The clinical isolates had varying susceptibility against well-established antimicrobials (Carbapenem and Colistin) as determined by the automated VITEK 2 C system (Biomeriux, France) and are given in Table 1. Clinical strain 2 was a multidrug-resistant (MDR) strain, resistant even to Colistin, often the last resort treatment for MDR infections, while clinical strain 3 was a highly susceptible strain, susceptible even to lower antibiotics.

https://doi.org/10.1021/acsomega.1c06398
ACS Omega 2022, 7, 6795−6809

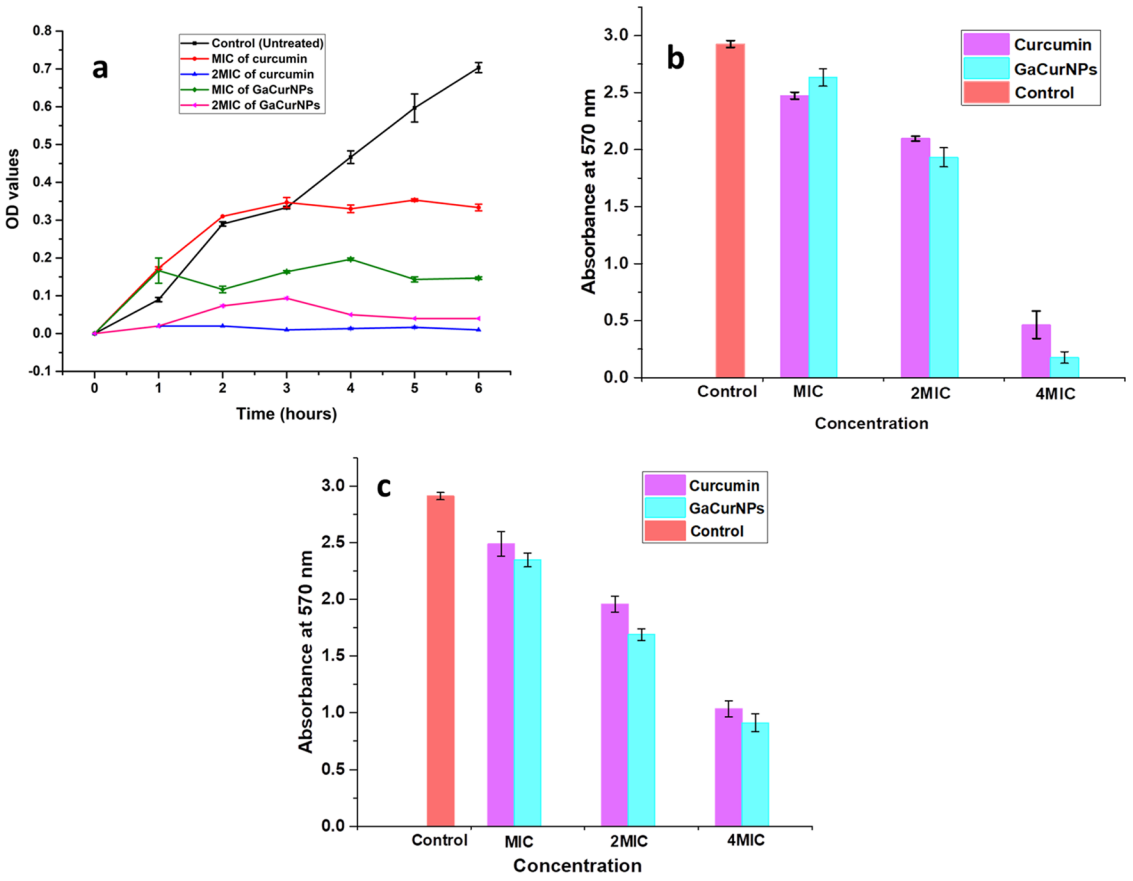

Figure 6. (a) Growth curves of *P. aeruginosa* (ATCC 27853) after treating with curcumin and GaCurNPs and without treatment; (b) effect of MIC, 2MIC, and 4MIC of curcumin and GaCurNPs on the biofilm formation of *P. aeruginosa*; and (c) effect of different concentrations of curcumin and GaCurNPs on the mature biofilm of *P. aeruginosa*.

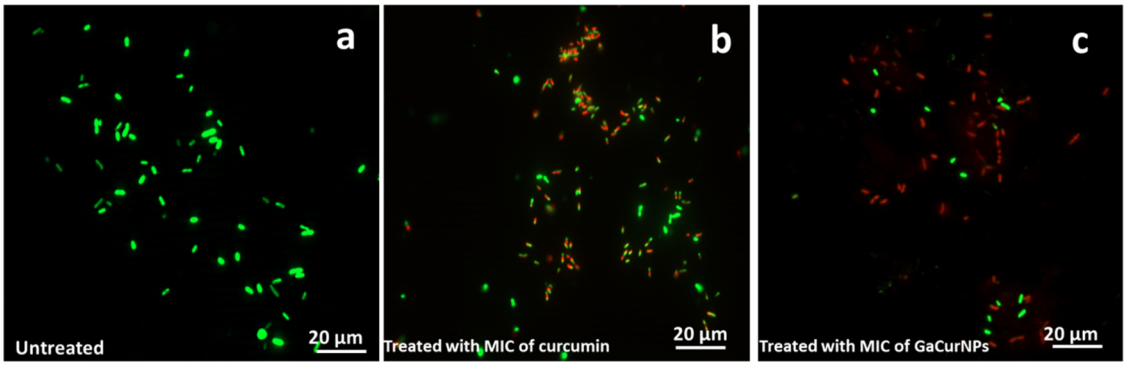

Figure 7. Fluorescence microscopy images of (a) untreated *P. aeruginosa*, (b) *P. aeruginosa* treated with the MIC of Curcumin, and (c) *P. aeruginosa* treated with the MIC of GaCurNPs. Live cells appear green, and dead cells appear red.

The promising results of the MIC experiments on *P. aeruginosa* merit further detailed studies to determine their antibacterial efficacy against its different clinically isolated strains.

2.7.2. Growth Curve of P. aeruginosa on Treatment with GaCurNPs. *P. aeruginosa* (ATCC 27853) was treated with MIC and 2MIC of GaCurNPs and curcumin. The OD values were taken every hour for 6 h, starting from the 0th h. Figure 6a shows a typical growth curve obtained, and it can be seen that the OD values of untreated *P. aeruginosa* increased in a linear fashion, whereas the bacteria treated with GaCurNPs and curcumin showed a decline. *P. aeruginosa* treated with MIC of GaCurNPs initially showed an increase in OD due to the growth of bacteria, which later declined, indicating its antibacterial activity. The increase in OD may be related to the time taken by curcumin/nanoparticles to enter the bacterial cell and to initiate cell lysis. These results are in agreement with the scanning electron microscopy (SEM) analysis (Section 2.7.6). When treating with the MIC of curcumin, interestingly, the OD initially showed an increasing trend till 3rd h and then stabilized. In the case of nanoparticles, faster lysis might be occurring. Curcumin showed its activity only after 3 h of treatment. When the bacteria were subjected to the 2MIC of curcumin, growth was totally inhibited (Figure 6a).

2.7.3. Effect of GaCurNPs on Biofilm Formation and Mature Biofilms. Curcumin is known to inhibit the formation of biofilms of *P. aeruginosa* by downregulating the genes

https://doi.org/10.1021/acsomega.1c06398
ACS Omega 2022, 7, 6795−6809

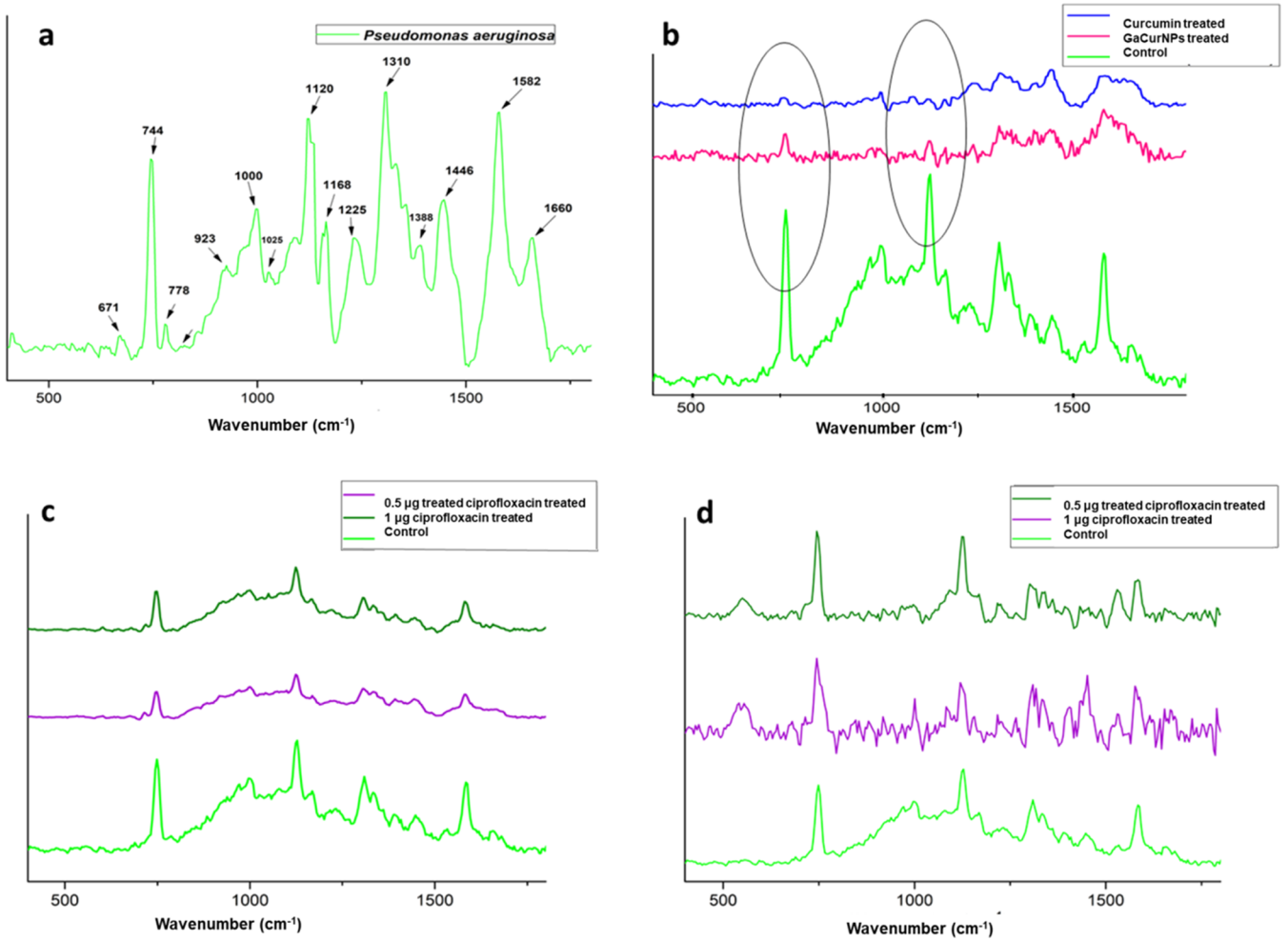

Figure 8. Raman spectra of (a) untreated *P. aeruginosa* (i.e., control), (b) *P. aeruginosa* treated with curcumin and GaCurNPs for 3 h, (c) *P. aeruginosa* treated with ciprofloxacin for 3 h, and (d) *P. aeruginosa* treated with ciprofloxacin for 24 h.

associated with it.[49] The effect of different concentrations of GaCurNPs on the inhibition of biofilm formed by *P. aeruginosa* was assessed using the crystal violet assay, and the results are shown in Figure 6b. An untreated biofilm is shown as a control. Biofilm inhibition was 10.03% when treated with the MIC of GaCurNPs, but when the concentration was quadrupled (331 μg/mL), a very significant reduction of 93.95% was observed. On the other hand, the reduction achieved with the 4MIC of curcumin was 84.08%, indicating the better inhibitory action of GaCurNPs at higher concentrations (Figure 6b).

The effect of GaCurNPs on the destruction of mature biofilms of *P. aeruginosa* is shown in Figure 6c. Our data shows that GaCurNPs are also effective in destroying the mature biofilm of *P. aeruginosa*. The MIC of GaCurNPs exhibited only 19.3% reduction, and twice the MIC showed a 41.97% reduction in the biofilm. When treated with 4MIC, the reduction was 69%. Complete destruction of the biofilm could not be achieved with the concentrations studied.

2.7.4. Live/Dead Assay. *P. aeruginosa* (ATCC 27853) was treated for 3 h with the MIC of GaCurNPs and curcumin, and the live/dead assay was performed on it. Fluorescence microscopy images showed that bacterial cells were viable/live in control/untreated *P. aeruginosa* (Figure 7a). Cells when treated with the MIC of GaCurNPs appeared red due to propidium iodide staining, which indicates that the integrity of the cell membrane was compromised (Figure 7c). This disruption of the cell membrane by GaCurNPs resulted in bacterial cell death at its MIC concentration. These results correlate well with the observations in growth curve estimation and Raman and SEM analyses. Bacterial cells treated with the MIC of curcumin showed fewer dead cells (Figure 7b) compared to GaCurNPs, implying that curcumin is showing its bactericidal action at a slightly slower pace than GaCurNPs.

2.7.5. Effect of GaCurNPs on P. aeruginosa: Raman Spectroscopy Evidence. Additional evidence on the antibacterial activity of curcumin and GaCurNPs against *P. aeruginosa* was obtained from Raman spectroscopy. Untreated *P. aeruginosa* was used as the control, and its Raman spectrum is shown in Figure 8a. Raman peaks were scattered from 500 to 1700 cm^{-1} (Table S1). The strong peak at 744 cm^{-1} was of wagging vibration of *l*-tryptophan, whereas the one at 671 cm^{-1} was indicative of hydrophobic amino acid valine. The uracil, cytosine, and thymine ring breathing peak was obtained at 778 cm^{-1}. Wavenumber 1000 cm^{-1} refers to phenylalanine and the C−C stretching of glycosidic linkage, while C−O−C skeletal stretching contributes to the peak at 1120 cm^{-1}. The amide II peak and amide I peak were obtained at 1582 and 1660 cm^{-1}, respectively.[50,51]

P. aeruginosa is rich in outer membrane porins, which are antiparallel β-sheets. The porin structure is such that the hydrophobic amino acids are exposed to the outside. The strong peak at 744 cm^{-1} was suggestive of tryptophan, which is

https://doi.org/10.1021/acsomega.1c06398
ACS Omega 2022, 7, 6795−6809

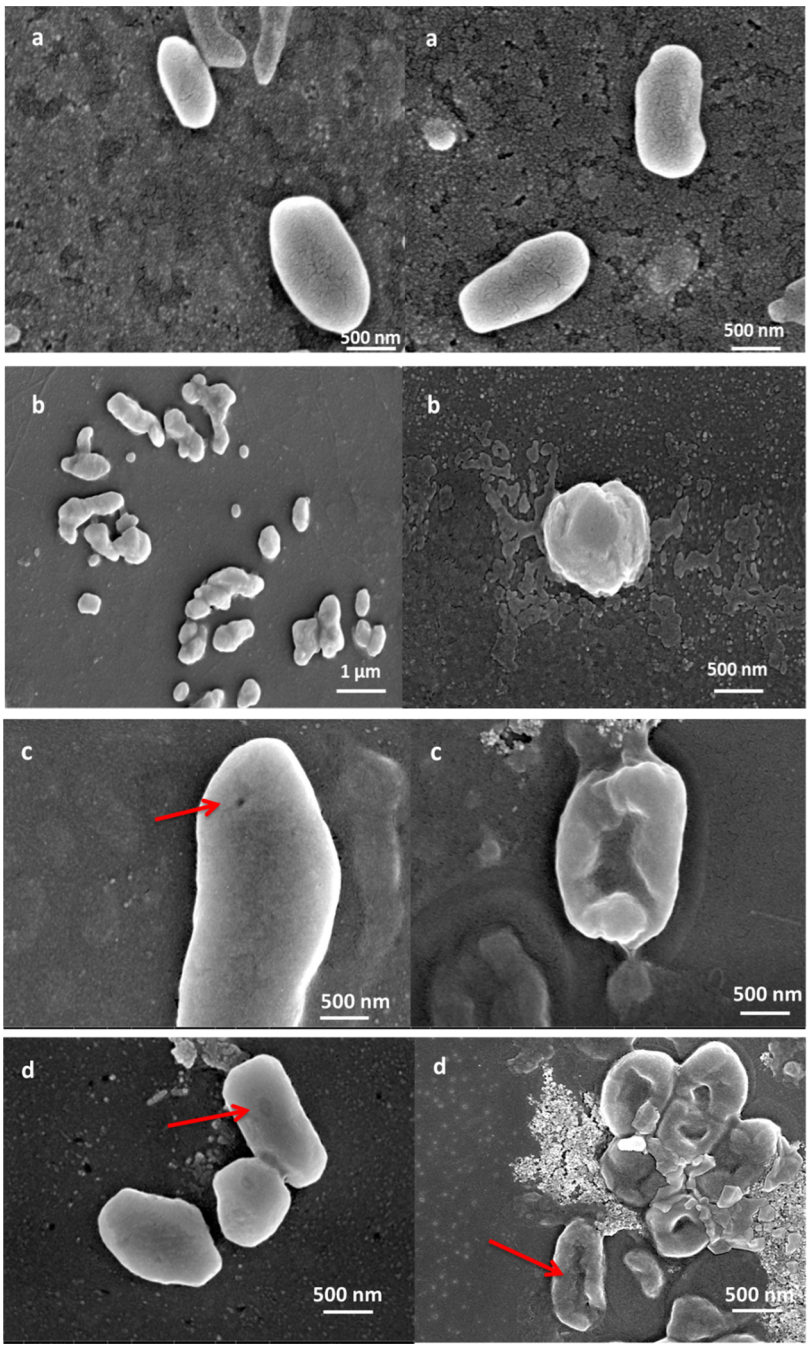

Figure 9. FESEM images of (a) untreated *P. Aeruginosa*, (b) *P. aeruginosa* treated with the MIC of ciprofloxacin for 3 h, (c) *P. aeruginosa* treated with the MIC of curcumin for 3 h, and (d) *P. aeruginosa* treated with the MIC of GaCurNPs for 3 h.

a hydrophobic amino acid. The peak at 671 cm^{-1} refers to valine stretching vibration, which is also hydrophobic. Notable differences can be seen in the spectra of curcumin- and GaCurNP-treated *P. aeruginosa* in comparison with the control. The Raman peaks of GaCurNP-treated *P. aeruginosa* were more resolved compared to those of curcumin-treated bacteria. The antibacterial action of curcumin against *P. aeruginosa* PA01 was found to be by the downregulation of the biofilm initiation gene.[49] On comparing the Raman peaks of curcumin-treated and GaCurNP-treated bacteria, the major difference found was between the two peaks at 744 and 1125 cm^{-1}, whereas both the peaks were diminished greatly in curcumin-treated bacteria. The difference in the 1125 cm^{-1} peak, which is contributed by the C−O stretching of saccharide, correlates with the results observed by Rudrappa et al.[49] Possibly the downregulation of genes associated with biofilm formation resulted in a reduction in the production of saccharide, which may be the action of curcumin on *P. aeruginosa*. The peaks are more resolved in the curcumin-treated system compared to the GaCurNP-treated system. In GaCurNPs, the peaks are weak and unresolved, suggesting the increased activity of GaCurNPs. The antibacterial activity of curcumin appears to be bacterial strain-specific, as reported by independent research groups. The activity of curcumin is reported to be associated with disruption of membranes of *S. aureus*, *E. coli*, *P. aeruginosa*, and *Enterococcus faecalis*.[25] In *B.*

https://doi.org/10.1021/acsomega.1c06398
ACS Omega 2022, 7, 6795−6809

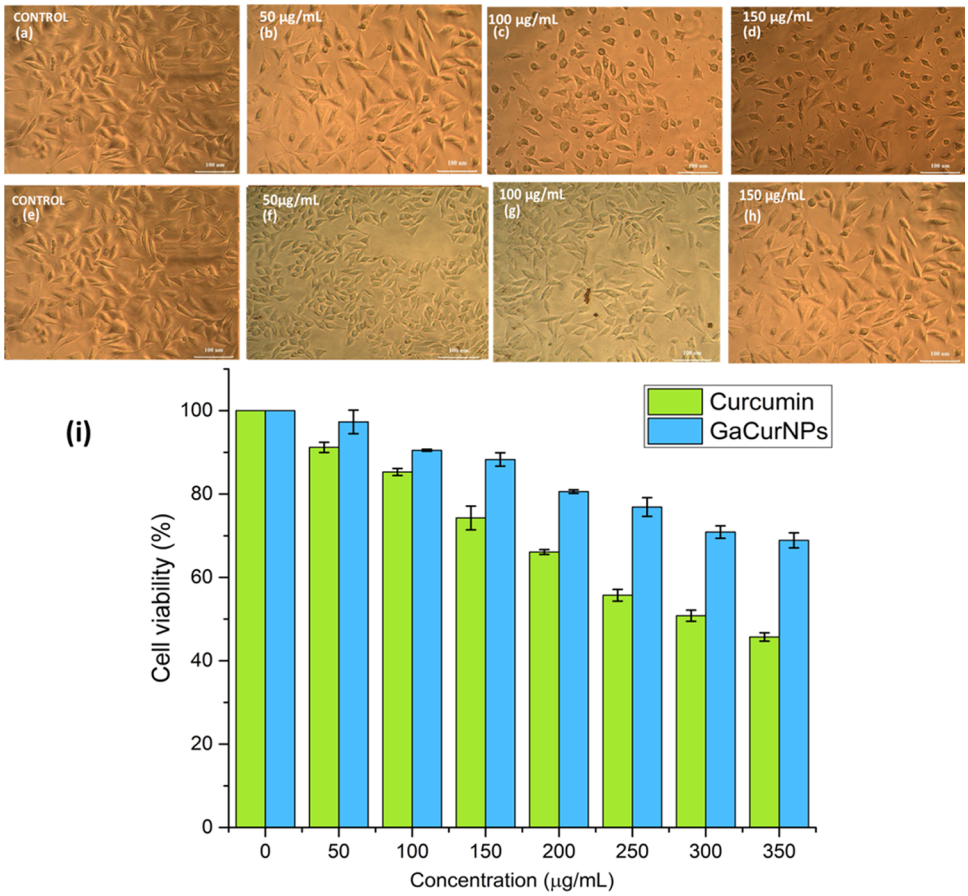

Figure 10. (a–h) Phase-contrast images showing the effect of GaCurNPs and curcumin on L929 cell lines; (a) and (e) control—untreated L929 cells; (b–d) L929 cells treated with curcumin with concentrations 50, 100, and 150 μg/mL for 24 h, respectively; (f–h) L929 cells treated with GaCurNPs having curcumin concentrations 50,100, and 150 μg/mL; and (i) effect of different concentrations of curcumin and GaCurNPs on the viability of L929 cell lines quantified by the AlamarBlue assay.

subtilis, curcumin inhibits cytokinesis by inhibiting the Z-ring formation.[52] The disruption of the membrane will lead to leakage of all cell contents. There is a drastic reduction in the 2927 cm^{-1} $-CH_2$ peak in both curcumin-treated and GaCurNP-treated systems, which suggested the disintegration and rupture of the cell membrane. The peaks at 1309 cm^{-1}, contributed by the CH groups, are also shattered in both treated samples, suggesting bacterial membrane damage.

For nanoparticles to be effective, their size should be less than 50 nm.[53] The antibacterial activity of silver nanoparticles is due to their smaller particle size that possesses superior penetration ability into bacteria, especially in Gram-negative bacteria.[54] In the case of GaCurNPs, their sizes were less than 50 nm. As a result, the action due to the size of nanoparticles as well as the inherent activity by the bound curcumin can be expected. Nanoparticles exert their action by permeating the cell membrane and entering the cell.[24] The antibacterial activity exhibited by nanoparticles, after their entry into bacterial cells, was reported to be due to ROS production or their interaction with intracellular components like DNA and proteins, leading to leakage of cell contents.[55] The Raman peaks obtained (Figure 8b) are almost unrecognizable and nonresolved, suggesting the substantial damage that happened to the cell structure of *P. aeruginosa* by the action of GaCurNPs. It may be noted that GaCurNPs could exhibit their antibacterial activity within 3 h of physical contact with bacteria in the physiological conditions. On the other hand, treatment with MIC of ciprofloxacin did not show much change in the Raman spectral features, indicating that its effect was not substantial when the contact with the bacteria was only 3 h (Figure 8c). Ciprofloxacin is a fluoroquinolone drug that covalently binds to topoisomerase IV and DNA gyrase.[56] In ciprofloxacin-treated (both 0.5 and 1 μg/mL) sample, the Raman spectral features were comparable to those of control bacteria (Figure 8c). When the bacteria were treated with ciprofloxacin for 24 h, we could see a substantial change in the spectral features, implying the destruction of bacterial cell structure (Figure 8d). We got comparable responses when *P. aeruginosa* was treated with GaCurNPs for 3 h and ciprofloxacin for 24 h. Further evidence of bacterial damage was obtained from SEM and is discussed in the next section.

2.7.6. Effect of GaCurNPs on P. aeruginosa: Observations under Field-Emission Scanning Electron Microscopy (FESEM). *P. aeruginosa* treated with MICs of GaCurNPs, curcumin, and ciprofloxacin were imaged using FESEM to ratify the results obtained by Raman spectroscopy. Untreated *P. aeruginosa* was used as the control (Figure 9a). The membrane damaging property of GaCurNPs is evident from the SEM images (Figure 9d). The size of the nanoparticles plays a major role in antibacterial activity, i.e., smaller nanoparticles elicit better antibacterial activity.[57] The particle size observed for GaCurNPs was 25–35 nm, and therefore, the activity may be inferred to be better. In the case of GaCurNPs, the activity elicited was the activity of nanoparticles' as well as

https://doi.org/10.1021/acsomega.1c06398
ACS Omega 2022, 7, 6795–6809

curcumin. The GaCurNPs might be entering the cells, causing cell membrane damage, leading to oozing out of cell contents. In Figure 9d, i.e., in GaCurNP-treated bacteria, we can clearly visualize the complete destruction of the bacterial cell structure and oozing out of cell components. Crater/dent formation can also be seen in GaCurNP-treated bacteria. It is noteworthy that the activity of GaCurNPs is elicited within a very short period of time, i.e., 3 h of incubation.

The bacterial membrane damaging property of curcumin (termed curcumin I) was reported by Tyagi et al. with supporting SEM images.[25] The results we obtained concur with the existing literature. When the bacterial cells were treated with curcumin (Figure 9c), there was dent/crater formation on the surface, which suggests membrane destruction. In the case of ciprofloxacin-treated bacteria (Figure 9b), the bacterial morphological features were different from those of nanoparticle- and curcumin-treated systems. In Figure 9b, some cells can be seen to be in a transition to become 'ovoid cells' and some were already close to a spherical shape, which is a characteristic feature observed in bacteria treated with ciprofloxacin. It has been reported that ciprofloxacin treatment results in pleated cell wall and shrinkage of cells, which is also evident from Figure 9b.[58]

GaCurNPs exhibited a quick and superior cell-damaging effect on *P. aeruginosa* and caused complete destruction of the cells when compared to ciprofloxacin, and this happened in just 3 h of contact.

2.8. Cytotoxicity of GaCurNPs on the L929 Cell Line. Cytotoxicity of GaCurNPs on the L929 cell line was analyzed using a phase-contrast microscope (Figure 10). The cytotoxic effects of curcumin on the L929 cell line were evident from the phase-contrast images. After 24 h of incubation, curcumin showed no cytotoxicity at 50 μg/mL concentration. At 100 μg/mL, curcumin started showing cytotoxicity and the morphology of the cells changed owing to the toxicity. On the other hand, GaCurNPs did not exhibit any considerable/significant cytotoxicity at 100 μg/mL after incubation for 24 h. At 150 μg/mL GaCurNPs also, the cells were in normal morphology and very few numbers of nonviable cells can be seen. Viability of cells is more in 100 and 150 μg/mL of GaCurNPs treatment when compared to curcumin treatment. The cytotoxic IC_{50} value of curcumin against the HEK cell line was reported by Adahoun *et al.* as 458.14 μM, which coincides with the results obtained.[59] GaCurNPs are noncytotoxic even at a concentration greater than its MIC values. Therefore, it can safely be used topically for antibacterial applications.

The cytotoxicity of GaCurNPs was further assessed by the AlamarBlue assay. AlamarBlue is a blue nonfluorescent dye that would be reduced to pink, highly fluorescent resorufin and is useful in monitoring the reducing environment of the living cells. The increase in dead cells lowers the ability of cells to convert resazurin to resorufin, which can be correlated to the decrease in fluorescent intensity. The effect of different concentrations of curcumin and GaCurNPs on the cell viability of L929 cell lines is depicted in Figure 10i. When the concentration of GaCurNPs was 250 μg/mL, the cell viability obtained was 76.9%, and it was higher than the viability of cells treated with the same concentration of curcumin. When the concentration of GaCurNPs was 350 μg/mL, the cells exhibited 68.9% viability, whereas 45.7% viability was shown with curcumin at the same concentration. At a concentration of 100 μg/mL, which is close to the MIC of GaCurNPs (82.75 μg/mL), about 90% cell viability was observed. GaCurNPs showed lower cytotoxicity than curcumin at all concentrations tested. Even at 4MIC concentration, where GaCurNPs inhibited 93.9% biofilm, the cell viability was about 69%, indicating that the material is safe to use at high doses.

3. CONCLUSIONS

In this study, we report a novel Gallium−Curcumin nanoparticle as a chemotherapeutic agent against pathogenic bacteria *P. aeruginosa*. This is the first reported green synthesis and characterization of GaCurNPs with improved curcumin stability and excellent antibacterial activity against clinically relevant pathogens. The GaCurNPs had spherical morphology and were of size 25−35 nm. The interaction between gallium and curcumin was elucidated by IR spectroscopy, Raman spectroscopy, and XPS. Curcumin bound to the GaCurNPs was found to be stable in physiological pH conditions up to 24 h with the degradation of 23.4%, which is clinically useful. GaCurNPs showed promising antibacterial activity against *P. aeruginosa*. These nanoparticles appear to be promising candidates for use as a fast-action antibacterial agent for topical applications. Also, the excellent antibacterial activity can be explored for treating hospital-acquired infections caused by *P. aeruginosa*. Improved stability of curcumin attached to GaCurNPs and its antibacterial activity makes it a potential choice as coatings on biomedical devices and also for healing chronic wounds infected with bacterial biofilms.

4. EXPERIMENTAL SECTION

4.1. Materials. Curcumin, trade name Biocurcumin/BCM, used for this study was obtained from Arjuna Natural Extracts Ltd., Aluva, Kerala, India. Gallium chloride (purity ≥ 99.99%) was purchased from Sigma-Aldrich. Ethanol (99.9%) was procured from SD Fine Chemicals, Mumbai. Tetrahydrofuran (HPLC grade) was purchased from Spectrochem Pvt. Ltd., Mumbai. Citric acid was obtained from Central Drug House Pvt. Ltd., New Delhi. *P. aeruginosa* (ATCC 27853) was obtained from ATCC. Ciprofloxacin, Luria broth, and Muller−Hinton broth were purchased from HiMedia Laboratories Pvt. Ltd., Mumbai. Milli-Q water was used for the synthesis and for all of the experiments conducted.

4.2. Synthesis of GaCurNPs. GaCurNPs were synthesized by following a simple procedure devoid of any reducing agent. For this, 500 μL of ethanolic solution of curcumin (concentration = 4 mg/mL) was added slowly to an RB flask containing 0.2 mM gallium chloride in 100 mL of Milli-Q water at room temperature. The reaction was monitored under dark conditions for 48 h. The color of the reaction mixture turned to greenish-yellow on the formation of the GaCurNPs. The unreacted reactants were removed by pressure filtration through the Biomax100 kDa ultrafiltration PES membrane. The resulting solution was used for dynamic light scattering, transmission electron microscopy, and antibacterial studies. The lyophilized powder was used for chemical characterization.

4.3. Characterization of GaCurNPs. *4.3.1. Size and ζ-potential.* The hydrodynamic diameters and the ζ-potentials of the synthesized GaCurNPs in the aqueous suspension were measured using Malvern Zetasizer Nano (Malvern Instruments, U.K.). The temperature was kept constant at 25 °C during the measurement.

https://doi.org/10.1021/acsomega.1c06398
ACS Omega 2022, 7, 6795−6809

4.3.2. Transmission Electron Microscopy. Morphological features of the GaCurNPs were studied using a transmission electron microscope (TEM) (Hitachi H-7650). A drop of the sample was allowed to air dry on carbon-coated copper grids. High-resolution TEM imaging was done using a JOEL JEM-2100, and the procedure adopted for sample preparation was the same as that mentioned above.

4.3.3. FT-IR Spectroscopy. FT-IR spectra of curcumin and GaCurNPs were recorded on a Nicolet 5700 (Thermo Fisher Scientific) spectrophotometer. The scanning range used was 400−4000 cm^{-1}. The KBr pellet method was employed for obtaining the spectra.

4.3.4. Raman Spectroscopy. Raman spectra of curcumin and GaCurNPs were recorded using a Confocal Raman Microscope (Alpha300 RA, WITec GmbH, Germany) using an excitation wavelength of 785 nm. All measurements were performed at room temperature (25 °C).

4.3.5. X-ray Photoelectron Spectroscopy. Elemental analysis was performed using X-ray photoelectron spectroscopy. The spectra were recorded by PHI500 Versa Probe II (ULVAC-PHI Inc.) equipped with a microfocused (200 μm, 15 kV) monochromatic Al Kα X-ray source ($h\nu$ = 148.6 eV). First survey scans were acquired on the sample, and for the major elements detected, high-resolution spectra were recorded. These spectra were used for estimating elemental composition (% atom) and chemical state assignment by curve fitting software. Survey scans were recorded with an X-ray source power of 23.7 W and a pass energy of 187.85 eV. High-resolution spectra of the major elements were recorded at 46.95 eV pass energy.

4.4. Estimation of Curcumin Content in GaCurNPs. The amount of curcumin per milligram of lyophilized GaCurNPs was quantified using reverse-phase high-performance liquid chromatography, RP-HPLC (LC-2010A, HT, Shimadzu, Japan). The C-18 column was used for the analysis. Citric acid solution (1%) and tetrahydrofuran in the ratio 60:40 was the solvent system used with an isocratic flow rate of 0.7 mL/min at an oven temperature of 30 °C. The data was analyzed using LC solution software. The injection volume was 20 μL, and the curcuminoids were detected at a wavelength of 420 nm. A calibration curve was plotted with the peak area of standard curcumin solutions against their concentrations ranging from 3.125 to 100 μg/mL. The calibration curve with a regression coefficient R^2 = 0.994 was used for the quantification of the curcumin content in GaCurNPs.

4.5. Stability of Curcumin in GaCurNPs. The curcumin bound to the GaCurNPs was analyzed for its stability by RP-HPLC. Curcumin and GaCurNPs were incubated in phosphate-buffered saline (PBS) at 37 °C for 24 h at 80 rpm in a shaker incubator. The sample was collected every hour till the 6th h and then at 24 h. The curcumin was then extracted by ethanol and loaded into HPLC. The degradation (%) of curcumin was estimated using the formula:

$$\text{degradation (\%)} = \frac{A_0 - A_n}{A_0} \times 100$$

where A_0 = area under the curve at the 0th hour and A_n = area under the curve at the nth hour.

4.6. Antibacterial Studies of GaCurNPs. *4.6.1. Determination of Minimum Inhibitory Concentration (MIC) and Minimum Bactericidal Concentration (MBC) of GaCurNPs.* The *in vitro* antibacterial activity of GaCurNPs and curcumin against *P. aeruginosa* (ATCC 27853) was evaluated by the microbroth dilution method. The broth dilution assay was done in 96-well microtiter plates. Bacteria were cultured in Mueller−Hinton broth, and the growth was adjusted to 0.5 McFarlands standard (1.5×10^8 CFU/mL). Subsequently, 200 μL of the stock solution of curcumin was added to the first well and then serially diluted and the same was done for GaCurNPs (a curcumin stock solution of 4 mg/mL was prepared and then diluted in autoclaved water to make a working stock of 662 μg/mL). The concentrations tested were 662, 331, 165.5, 82.75, 41.37, 20.68, and 10.34 μg/mL. In the case of clinical strains, we tested the concentrations starting from 400 to 25 μg/mL. About 100 μL of microbial inoculum (5×10^6 CFU/mL) was added to each well. Drug and organism controls were kept for each of the drug concentrations in triplicates. The plates were incubated at 37 °C for 24 h. MIC was determined as per the Clinical and Laboratory Standards Institute (CLSI) guidelines. MIC was the concentration at which the wells were clear, i.e., no visible turbidity. MBC was determined as the lowest concentration at which there was no appearance of colonies when transferred from broth to agar plates.

4.6.2. Growth Curve of P. aeruginosa Treated with GaCurNPs. About 2.5 mL each of Luria−Bertani (LB) broth was taken in test tubes. The GaCurNP suspension (taken from the stock) was added to these test tubes, and their concentrations were adjusted to get MIC and 2MIC. Similarly, MIC and 2MIC of curcumin were also prepared. About 50 μL of 0.1 OD bacterial inoculum (freshly grown in 3−4 mL of LB broth) was added to these test tubes. The tubes were then incubated at 37 °C. The OD_{600} readings were taken every hour for 6 h starting from 0th h. The control tube, which was untreated *P. aeruginosa*, was also kept along with the treated bacteria. Data was plotted with OD_{600} values on the *Y*-axis and time on the *X*-axis.

4.6.3. Effect of GaCurNPs on P. aeruginosa Biofilms by the Crystal Violet Assay. *P. aeruginosa* (ATCC 27853) was inoculated in 3−5 mL of LB broth and grown to the stationary phase. The culture was diluted 1:100 in LB broth. A 96-well plate was used for the assay. From the diluted culture, 100 μL of volume was taken and added to each well. The bacterial cells were treated with MIC, 2MIC, and 4MIC of GaCurNPs. The procedure was also done for curcumin. Untreated cells were kept as the control. The plate was incubated at 37 °C for 48 h undisturbed to form the biofilm. After 48 h, the plate was taken out and planktonic cells were washed with water. The cells were heat-fixed at 60 °C for 60 min.[60] About 125 μL of crystal violet dye was added to wells and kept at room temperature for 15 min for the biofilm to get stained. The wells were then washed with water to remove excess stain and dried. About 200 μL of 30% acetic acid was added to the wells. The OD values were measured at 570 nm in a microplate reader (Biotek 800 TS, VT). The inhibition (%) of the biofilm was calculated using the following formula:

$$\text{biofilm inhibiton (\%)} = \frac{\text{OD (control) at 570 nm} - \text{OD (treated) at 570 nm}}{\text{OD (control) at 570 nm}} \times 100$$

The effect of GaCurNPs on the mature biofilm was also studied. After growing the *P. aeruginosa* biofilm for 48 h, the biofilm was treated with MIC, 2MIC, and 4MIC of GaCurNPs. The procedure was also done for curcumin. The untreated biofilm was kept as the control. The treated biofilms were kept

https://doi.org/10.1021/acsomega.1c06398
ACS Omega 2022, 7, 6795−6809

for 24 h, and the crystal violet assay was performed. Degradation of the biofilm (%) was calculated using the above equation.

4.6.4. Live/Dead Assay. The activity of GaCurNPs was assessed using the BacLight Live/Dead assay kit. Bacterial cells were treated with MICs of GaCurNPs and curcumin for 3 h. Untreated cells were kept as the control. Cells were collected by centrifugation at 10 000 rpm for 5 min. The cells were then washed with saline four times and resuspended in 250 μL of saline. They were then stained with SYTO9 and propidium iodide by adding 3 μL of staining solution (equal volumes of SYTO9 and propidium iodide, mixed and vortexed). After this, cells were incubated for 15 min in the dark. About 5 μL of the solution was placed on a glass slide, and a coverslip was mounted on the top. Using an inverted fluorescence microscope (Zeiss Axio Vert A1, Germany), the live/dead cells were observed and imaged. Live cells appeared green, and dead cells appeared red. The excitation/emission maximum of SYTO9 was 480/500 nm, and that of propidium iodide was 490/635 nm.

4.7. Effect of GaCurNPs on *P. aeruginosa* Using Raman Spectroscopy. The antibacterial activity of GaCurNPs against *P. aeruginosa* was further investigated by Raman spectroscopy. One milliliter of 16 h culture of *P. aeruginosa* was freshly inoculated into Luria broth. Cells were collected by centrifuging at 10 000 rpm for 5 min and then diluted to reach 0.5 OD. Bacteria were treated with MIC concentrations of GaCurNPs and curcumin for 3 h. Bacteria were also treated with ciprofloxacin (MIC, 0.5 μg/mL; 2MIC, 1 μg/mL) for 3 h.[61] Untreated bacteria were kept as the control. Bacterial cells were collected by centrifugation at 10 000 rpm for 5 min after incubation. Cells were resuspended in 3 μL of Milli-Q water and dropped on a calcium fluoride slide. After drying, Raman spectra were recorded. Raman spectra were acquired using a confocal Raman microscope equipped with 600 g/mm grating. Excitation was provided by a diode (DPSS) 785 nm laser with a power of 30mW applied to the sample. An acquisition time of 5 s was used. A 20× objective was used throughout the acquisition of spectra.

4.8. Effect of GaCurNPs on *P. aeruginosa* Using FESEM. The antibacterial activity of GaCurNPs against *P. aeruginosa* was further investigated by FESEM. Bacterial cells from a 16 h culture of *P. aeruginosa* were collected by centrifugation at 10 000 rpm for 5 min. Cells were then diluted to reach 0.5 OD. Bacteria were treated with the MICs of ciprofloxacin, GaCurNPs, and curcumin for 3 h in PBS (pH 7.5). Untreated bacteria were kept as the control. Bacterial cells were centrifuged at 10 000 rpm for 5 min at the end of the incubation period and subsequently resuspended in 1 mL of Milli-Q water. The bacterial suspension was dropped on a coverslip and dried. The samples were sputter-coated with gold for 20 s, and images were obtained using a Nova NanoSEM 450.

4.9. Cytotoxicity of GaCurNPs on the L929 Cell Line. The cell line was cultured in a 25 cm^2 tissue culture flask with DMEM supplemented with 10% FBS, L-glutamine, sodium bicarbonate (Merck, Germany), and an antibiotic solution containing penicillin (100 U/mL), streptomycin (100 μg/mL), and amphotericin B (2.5 μg/mL). Cultured cell lines were kept at 37 °C in a humidified 5% CO_2 incubator (NBS Eppendorf, Germany). A 2 day old confluent monolayer of cells was trypsinized, and the cells were suspended in a 10% growth medium; 100 μL of cell suspension (5×10^3 cells/well) was seeded in 96-well tissue culture plate and incubated at 37 °C in a humidified 5% CO_2 incubator. After 24 h, the growth medium was removed, and cells were treated with different concentrations of curcumin and GaCurNPs (50, 100, and 150 μg/mL). From each of the above concentrations, 100 μL was taken and added to the respective wells and incubated at 37 °C in a humidified 5% CO_2 incubator for 24 h. Experiments were done in triplicate. Nontreated cells were also maintained and used as the control. Phase-contrast images of cells were taken for each of these concentrations using an inverted microscope.

A quantitative assessment of the cytotoxicity of GaCurNPs toward L929 fibroblast cell lines was done by the AlamarBlue assay. For this, the 2 day old confluent monolayer of cells was trypsinized and the cells were suspended in a 10% growth medium. About 100 μL of cell suspension (5×10^3 cells/well) was seeded in a 96-well tissue culture plate and incubated at 37 °C in a humidified 5% CO_2 incubator. After 24 h, the growth medium was removed and the cells were treated with different concentrations of curcumin/GaCurNPs (100, 50, 25, 12.5, 6.25 μg). About 100 μL of each concentration was added in triplicate to the respective wells and incubated at 37 °C in a humidified 5% CO_2 incubator for 24 h. Nontreated cells were also maintained and used as the control. After 24 h treatment, 10 μL of the Alamar reagent was added to the treated cells in the media. The cells were incubated for 4 h at 37 °C in a humidified 5% CO_2 incubator. The fluorescence was measured using a fluorimeter (Qubit 3.0, Life Technologies) at an excitation wavelength of 530−560 nm and emission wavelength of 590 nm. The cell viability (%) was calculated using the formula:

$$\text{cell viability (\%)} = \frac{\text{mean fluorescence intensity of treated sample}}{\text{mean fluorescence intensity of control}} \times 100$$

■ ASSOCIATED CONTENT

Supporting Information

The Supporting Information is available free of charge at https://pubs.acs.org/doi/10.1021/acsomega.1c06398.

Characteristic Raman peaks of *Pseudomonas aeruginosa* and comparison of MIC values of curcumin obtained from the literature (PDF)

■ AUTHOR INFORMATION

Corresponding Author

Roy Joseph − *Division of Polymeric Medical Devices, Department of Medical Devices Engineering, Biomedical Technology Wing, Sree Chitra Tirunal Institute for Medical Sciences and Technology, Trivandrum 695012 Kerala, India;* orcid.org/0000-0002-4828-3586; Phone: 0471 2520275; Email: rjoseph@sctimst.ac.in

Authors

Gopika Ramesh − *Division of Polymeric Medical Devices, Department of Medical Devices Engineering, Biomedical Technology Wing, Sree Chitra Tirunal Institute for Medical Sciences and Technology, Trivandrum 695012 Kerala, India*

Jyothi Embekkat Kaviyil − *Department of Microbiology, Sree Chitra Tirunal Institute for Medical Sciences and Technology, Trivandrum 695011 Kerala, India*

Willi Paul − *Central Analytical Facility, Department of Technology and Quality Management, Biomedical*

https://doi.org/10.1021/acsomega.1c06398
ACS Omega 2022, 7, 6795−6809

Technology Wing, Sree Chitra Tirunal Institute for Medical Sciences and Technology, Trivandrum 695012 Kerala, India

Renjith Sasi − *Central Analytical Facility, Department of Technology and Quality Management, Biomedical Technology Wing, Sree Chitra Tirunal Institute for Medical Sciences and Technology, Trivandrum 695012 Kerala, India;* orcid.org/0000-0002-6430-2556

Complete contact information is available at: https://pubs.acs.org/10.1021/acsomega.1c06398

Author Contributions

G.R., methodology, data curation, investigation, and writing—original draft. J.E.K., supervision of antibacterial studies and writing—review and editing. W.P., methodology, formal analysis, and visualization. R.S., formal analysis and writing—review and editing. R.J., supervision, conceptualization, writing—review and editing, visualization, and resources.

Notes

The authors declare no competing financial interest.

■ ACKNOWLEDGMENTS

The authors acknowledge the Director and the Head BMT Wing, SCTIMST, Trivandrum for the facilities extended and kind permission to publish this work. The authors also acknowledge Dr. Kavita Raja, a Professor and the Head of the Department of Microbiology, SCTIMST, for her kind permission to conduct the microbiology studies at her lab. Gopika Ramesh acknowledges the receipt of the DST-INSPIRE fellowship.

■ ABBREVIATIONS

P. aeruginosa, *Pseudomonas aeruginosa*; MIC, minimum inhibitory concentration; 2MIC, twice the MIC value; 4MIC, four times the MIC value; GaO(OH), gallium oxide hydroxide; DMEM, Dulbecco's modified Eagle's medium; TEM, transmission electron microscopy; LB broth, Luria−Bertani broth

■ REFERENCES

(1) Ventola, C. L. The Antibiotic Resistance Crisis. *Pharm. Ther.* **2015**, *40*, 277−283.
(2) Munita, J. M.; Arias, C. A. Mechanisms of Antibiotic Resistance. In *Virulence Mechanisms of Bacterial Pathogens*; John Wiley & Sons, Ltd, 2016; pp 481−511.
(3) Lambert, P. A. Mechanisms of Antibiotic Resistance in *Pseudomonas aeruginosa*. *J. R. Soc. Med.* **2002**, *95*, 22−26.
(4) Rahim, M. I.; Rohde, M.; Rais, B.; Seitz, J. M.; Mueller, P. P. Susceptibility of metallic magnesium implants to bacterial biofilm infections. *J. Biomed. Mater. Res., Part A* **2016**, *104*, 1489−1499.
(5) Ribeiro, M.; Monteiro, F. J.; Ferraz, M. P. Infection of Orthopedic Implants with Emphasis on Bacterial Adhesion Process and Techniques Used in Studying Bacterial-Material Interactions. *Biomatter* **2012**, *2*, 176−194.
(6) Hancock, R. E. W. Resistance Mechanisms in *Pseudomonas aeruginosa* and Other Nonfermentative Gram-Negative Bacteria. *Clin. Infect. Dis.* **1998**, *27*, S93−S99.
(7) Soheili, V.; Tajani, A. S.; Ghodsi, R.; Bazzaz, B. S. F. Anti-PqsR Compounds as next-Generation Antibacterial Agents against *Pseudomonas aeruginosa*: A Review. *Eur. J. Med. Chem.* **2019**, *172*, 26−35.
(8) Lee, J.-H.; Kim, Y.-G.; Cho, M. H.; Kim, J.-A.; Lee, J. 7-Fluoroindole as an Antivirulence Compound against *Pseudomonas aeruginosa*. *FEMS Microbiol. Lett.* **2012**, *329*, 36−44.
(9) Hibbard, H. A. J.; Reynolds, M. M. Fluorescent Nitric Oxide Donor for the Detection and Killing of *Pseudomonas aeruginosa*. *J. Mater. Chem. B* **2019**, *7*, 2009−2018.
(10) Liao, S.; Zhang, Y.; Pan, X.; Zhu, F.; Jiang, C.; Liu, Q.; Cheng, Z.; Dai, G.; Wu, G.; Wang, L.; Chen, L. Antibacterial Activity and Mechanism of Silver Nanoparticles against Multidrug-Resistant *Pseudomonas Aeruginosa*. *Int. J. Nanomed.* **2019**, *Volume 14*, 1469−1487.
(11) dos Santos, E. M. P.; Martins, C. C. B.; de Oliveira Santos, J. V.; da Silva, W. R. C.; Silva, S. B. C.; Pelagio-Flores, M. A.; Galembeck, A.; Cavalcanti, I. M. F. Silver Nanoparticles−Chitosan Composites Activity against Resistant Bacteria: Tolerance and Biofilm Inhibition. *J. Nanopart. Res.* **2021**, *23*, No. 196.
(12) Salomoni, R.; Léo, P.; Montemor, A.; Rinaldi, B.; Rodrigues, M. Antibacterial Effect of Silver Nanoparticles in *Pseudomonas aeruginosa*. *Nanotechnol. Sci. Appl.* **2017**, *Volume 10*, 115−121.
(13) Mitra, D.; Li, M.; Kang, E.-T.; Neoh, K. G. Transparent Copper-Based Antibacterial Coatings with Enhanced Efficacy against *Pseudomonas aeruginosa*. *ACS Appl. Mater. Interfaces* **2019**, *11*, 73−83.
(14) Negi, P. S.; Jayaprakasha, G. K.; Jagan Mohan Rao, L.; Sakariah, K. K. Antibacterial Activity of Turmeric Oil: A Byproduct from Curcumin Manufacture. *J. Agric. Food Chem.* **1999**, *47*, 4297−4300.
(15) Kuttan, R.; Bhanumathy, P.; Nirmala, K.; George, M. C. Potential Anticancer Activity of Turmeric (Curcuma Longa). *Cancer Lett.* **1985**, *29*, 197−202.
(16) Sharma, O. P. Antioxidant Activity of Curcumin and Related Compounds. *Biochem. Pharmacol.* **1976**, *25*, 1811−1812.
(17) Srimal, R. C.; Dhawan, B. N. Pharmacology of Diferuloyl Methane (Curcumin), a Non-Steroidal Anti-Inflammatory Agent. *J. Pharm. Pharmacol.* **2011**, *25*, 447−452.
(18) Zhang, L.; Fiala, M.; Cashman, J.; Sayre, J.; Espinosa, A.; Mahanian, M.; Zaghi, J.; Badmaev, V.; Graves, M. C.; Bernard, G.; Rosenthal, M. Curcuminoids Enhance Amyloid-β Uptake by Macrophages of Alzheimer's Disease Patients. *J. Alzheimer's Dis.* **2006**, *10*, 1−7.
(19) Lao, C. D.; Ruffin, M. T.; Normolle, D.; Heath, D. D.; Murray, S. I.; Bailey, J. M.; Boggs, M. E.; Crowell, J.; Rock, C. L.; Brenner, D. E. Dose Escalation of a Curcuminoid Formulation. *BMC Complementary Altern. Med.* **2006**, *6*, No. 10.
(20) Priyadarsini, K. I. The Chemistry of Curcumin: From Extraction to Therapeutic Agent. *Molecules* **2014**, *19*, 20091−20112.
(21) Li, M.; Xin, M.; Guo, C.; Lin, G.; Wu, X. New Nanomicelle Curcumin Formulation for Ocular Delivery: Improved Stability, Solubility, and Ocular Anti-Inflammatory Treatment. *Drug Dev. Ind. Pharm.* **2017**, *43*, 1846−1857.
(22) Sindhu, K.; Rajaram, A.; Sreeram, K. J.; Rajaram, R. Curcumin Conjugated Gold Nanoparticle Synthesis and Its Biocompatibility. *RSC Adv.* **2014**, *4*, 1808−1818.
(23) Jaiswal, S.; Mishra, P. Antimicrobial and Antibiofilm Activity of Curcumin-Silver Nanoparticles with Improved Stability and Selective Toxicity to Bacteria over Mammalian Cells. *Med. Microbiol. Immunol.* **2018**, *207*, 39−53.
(24) Bhawana; Basniwal, R. K.; Buttar, H. S. Curcumin Nanoparticles: Preparation, Characterization, and Antimicrobial Study. *J. Agric. Food Chem.* **2011**, *59*, 2056−2061.
(25) Tyagi, P.; Singh, M.; Kumari, H.; Kumari, A.; Mukhopadhyay, K. Bactericidal Activity of Curcumin I Is Associated with Damaging of Bacterial Membrane. *PLoS One* **2015**, *10*, No. e0121313.
(26) Gunes, H.; Gulen, D.; Mutlu, R.; Gumus, A.; Tas, T.; Topkaya, A. E. Antibacterial Effects of Curcumin: An in Vitro Minimum Inhibitory Concentration Study. *Toxicol. Ind. Health* **2016**, *32*, 246−250.
(27) Groundwater, P. W.; Narlawar, R.; Liao, V. W. Y.; Bhattacharya, A.; Srivastava, S.; Kunal, K.; Doddareddy, M.; Oza, P. M.; Mamidi, R.; Marrs, E. C. L.; Perry, J. D.; Hibbs, D. E.; Panda, D. A Carbocyclic Curcumin Inhibits Proliferation of Gram-Positive Bacteria by Targeting FtsZ. *Biochemistry* **2017**, *56*, 514−524.

(28) Liao, Y.; Yao, Y.; Yu, Y.; Zeng, Y. Enhanced Antibacterial Activity of Curcumin by Combination With Metal Ions. *Colloid Interface Sci. Commun.* **2018**, *25*, 1−6.
(29) Park, B.-S.; Kim, J.-G.; Kim, M.-R.; Lee, S.-E.; Takeoka, G. R.; Oh, K.-B.; Kim, J.-H. Curcuma Longa L. Constituents Inhibit Sortase A and *Staphylococcus Aureus* Cell Adhesion to Fibronectin. *J. Agric. Food Chem.* **2005**, *53*, 9005−9009.
(30) Khatoon, Z.; McTiernan, C. D.; Suuronen, E. J.; Mah, T.-F.; Alarcon, E. I. Bacterial Biofilm Formation on Implantable Devices and Approaches to Its Treatment and Prevention. *Heliyon* **2018**, *4*, e01067.
(31) Mohammadi, K.; Thompson, K. H.; Patrick, B. O.; Storr, T.; Martins, C.; Polishchuk, E.; Yuen, V. G.; McNeill, J. H.; Orvig, C. Synthesis and Characterization of Dual Function Vanadyl, Gallium and Indium Curcumin Complexes for Medicinal Applications. *J. Inorg. Biochem.* **2005**, *99*, 2217−2225.
(32) Rajasekar, A.; Devasena, T. Facile Synthesis of Curcumin Nanocrystals and Validation of Its Antioxidant Activity Against Circulatory Toxicity in Wistar Rats. *J. Nanosci. Nanotechnol.* **2015**, *15*, 4119−4125.
(33) Avivi, S.; Mastai, Y.; Hodes, G.; Gedanken, A. Sonochemical Hydrolysis of Ga3+ Ions: Synthesis of Scroll-like Cylindrical Nanoparticles of Gallium Oxide Hydroxide. *J. Am. Chem. Soc.* **1999**, *121*, 4196−4199.
(34) Adams, W. T.; Ivanisevic, A. Nanostructured Oxides Containing Ga: Materials with Unique Properties for Aqueous-Based Applications. *ACS Omega* **2019**, *4*, 6876−6882.
(35) Kolev, T. M.; Velcheva, E. A.; Stamboliyska, B. A.; Spiteller, M. DFT and Experimental Studies of the Structure and Vibrational Spectra of Curcumin. *Int. J. Quantum Chem.* **2005**, *102*, 1069−1079.
(36) Ganguly, B. N.; Verma, V.; Chatterjee, D.; Satpati, B.; Debnath, S.; Saha, P. Study of Gallium Oxide Nanoparticles Conjugated with β-Cyclodextrin: An Application To Combat Cancer. *ACS Appl. Mater. Interfaces* **2016**, *8*, 17127−17137.
(37) Zhao, Y.; Frost, R. L.; Yang, J.; Martens, W. N. Size and Morphology Control of Gallium Oxide Hydroxide GaO(OH), Nano- to Micro-Sized Particles by Soft-Chemistry Route without Surfactant. *J. Phys. Chem. C* **2008**, *112*, 3568−3579.
(38) Chen, X.; Zou, L.-Q.; Niu, J.; Liu, W.; Peng, S.-F.; Liu, C.-M. The Stability, Sustained Release and Cellular Antioxidant Activity of Curcumin Nanoliposomes. *Molecules* **2015**, *20*, 14293−14311.
(39) Nguyen, T. A.; Tang, Q. D.; Doan, D. C. T.; Dang, M. C. Micro and Nano Liposome Vesicles Containing Curcumin for a Drug Delivery System. *Adv. Nat. Sci.: Nanosci. Nanotechnol.* **2016**, *7*, No. 035003.
(40) Mohan, P. K.; Sreelakshmi, G.; Muraleedharan, C. V.; Joseph, R. Water Soluble Complexes of Curcumin with Cyclodextrins: Characterization by FT-Raman Spectroscopy. *Vib. Spectrosc.* **2012**, *62*, 77−84.
(41) Moussawi, R. N.; Patra, D. Nanoparticle Self-Assembled Grain Like Curcumin Conjugated ZnO: Curcumin Conjugation Enhances Removal of Perylene, Fluoranthene and Chrysene by ZnO. *Sci. Rep.* **2016**, *6*, No. 24565.
(42) Zhao, Y.; Frost, R. L. Raman Spectroscopy and Characterisation of α-Gallium Oxyhydroxide and β-Gallium Oxide Nanorods. *J. Raman Spectrosc.* **2008**, *39*, 1494−1501.
(43) Lee, E. J.; Hur, M. G.; Son, J. M.; Park, J. H.; Yang, S. D. Effect of Liquid Ga on Metal Surfaces: Characterization of Morphology and Chemical Composition of Metals Heated in Liquid Ga. *J. Nanomater.* **2013**, *2013*, 1−8.
(44) Bourque, J. L.; Biesinger, M. C.; Baines, K. M. Chemical State Determination of Molecular Gallium Compounds Using XPS. *Dalton Trans.* **2016**, *45*, 7678−7696.
(45) Feng, J.; Fu, B.; Fang, L.; Wang, F.; Zhang, X.; Li, Y.; Song, Y. Uniform Gallium Oxyhydroxide Nanorod Anodes with Superior Lithium-Ion Storage. *RSC Adv.* **2019**, *9*, 34896−34901.
(46) Kumavat, S. D.; Chaudhari, Y. S.; Borole, P.; Mishra, P.; Shenghani, K.; Duvvuri, P. Degradation Studies of Curcumin. *Int. J. Pharm. Rev. Res.* **2013**, *3*, 50−55.
(47) Yadav, S.; Singh, A. K.; Agrahari, A. K.; Sharma, K.; Singh, A. S.; Gupta, M. K.; Tiwari, V. K.; Prakash, P. Making of Water Soluble Curcumin to Potentiate Conventional Antimicrobials by Inducing Apoptosis-like Phenomena among Drug-Resistant Bacteria. *Sci. Rep.* **2020**, *10*, No. 14204.
(48) Roudashti, S.; Zeighami, H.; Mirshahabi, H.; Bahari, S.; Soltani, A.; Haghi, F. Synergistic Activity of Sub-Inhibitory Concentrations of Curcumin with Ceftazidime and Ciprofloxacin against *Pseudomonas aeruginosa* Quorum Sensing Related Genes and Virulence Traits. *World J. Microbiol. Biotechnol.* **2017**, *33*, No. 50.
(49) Rudrappa, T.; Bais, H. P. Curcumin, a Known Phenolic from Curcuma Longa, Attenuates the Virulence of *Pseudomonas Aeruginosa* PAO1 in Whole Plant and Animal Pathogenicity Models. *J. Agric. Food Chem.* **2008**, *56*, 1955−1962.
(50) Jung, G. B.; Nam, S. W.; Choi, S.; Lee, G.-J.; Park, H.-K. Evaluation of Antibiotic Effects on *Pseudomonas Aeruginosa* Biofilm Using Raman Spectroscopy and Multivariate Analysis. *Biomed. Opt. Express* **2014**, *5*, 3238.
(51) De Gelder, J.; Gussem, K. D.; Vandenabeele, P.; Moens, L. Reference Database of Raman Spectra of Biological Molecules. *J. Raman Spectrosc.* **2007**, *38*, 1133−1147.
(52) Rai, D.; Singh, J. K.; Roy, N.; Panda, D. Curcumin Inhibits FtsZ Assembly: An Attractive Mechanism for Its Antibacterial Activity. *Biochem. J.* **2008**, *410*, 147−155.
(53) Dakal, T. C.; Kumar, A.; Majumdar, R. S.; Yadav, V. Mechanistic Basis of Antimicrobial Actions of Silver Nanoparticles. *Front. Microbiol.* **2016**, *7*, 1831.
(54) Morones, J. R.; Elechiguerra, J. L.; Camacho, A.; Holt, K.; Kouri, J. B.; Ramírez, J. T.; Yacaman, M. J. The Bactericidal Effect of Silver Nanoparticles. *Nanotechnology* **2005**, *16*, 2346−2353.
(55) Wang, L.; Hu, C.; Shao, L. The Antimicrobial Activity of Nanoparticles: Present Situation and Prospects for the Future. *Int. J. Nanomed.* **2017**, *Volume 12*, 1227−1249.
(56) Hooper, D. C. Mode of Action of Fluoroquinolones. *Drugs* **1999**, *58*, 6−10.
(57) Karakoti, A. S.; Hench, L. L.; Seal, S. The Potential Toxicity of Nanomaterials—The Role of Surfaces. *JOM* **2006**, *58*, 77−82.
(58) Wojnicz, D.; Kłak, M.; Adamski, R.; Jankowski, S. Influence of Subinhibitory Concentrations of Amikacin and Ciprofloxacin on Morphology and Adherence Ability of Uropathogenic Strains. *Folia Microbiol.* **2007**, *52*, 429−436.
(59) Adahoun, M. A.; Al-Akhras, M.-A. H.; Jaafar, M. S.; Bououdina, M. Enhanced Anti-Cancer and Antimicrobial Activities of Curcumin Nanoparticles. *Artif. Cells, Nanomed., Biotechnol.* **2017**, *45*, 98−107.
(60) Kwasny, S. M.; Opperman, T. J. Static Biofilm Cultures of Gram-Positive Pathogens Grown in a Microtiter Format Used for Anti-Biofilm Drug Discovery. *Curr. Protoc. Pharmacol.* **2010**, *50*, 13A.8.1−13A.8.23.
(61) Patel, J. B. *Performance Standards for Antimicrobial Susceptibility Testing*; Clinical and Laboratory Standards Institute: Wayne, 2017.

https://doi.org/10.1021/acsomega.1c06398
ACS Omega 2022, 7, 6795−6809